Neural Maturation Stabilizes Representations and Supports Understanding of Complex Concepts

Hiroyasu. Watanabe[1]*,

Affiliations:

[1] Bream Research Group; Kyoto, 603-8081, Japan.

*Corresponding author. Email: bream@dontokois.net

Abstract:

Remarkable advances in AI do not necessarily rely on modern molecular biology. Here, I highlight the importance of neural maturation in neural network information processing. In both supervised and reinforcement learning, immature synaptic transmission can achieve high fidelity learning but suffers catastrophic failure beyond specific thresholds. I identified genes involved in neuronal maturation and found that the candidate gene KCNH7 is upregulated during mouse brain development. Incorporating KCNH7 channel properties into a simulated neural model raised the excitation threshold and yielded a more linear response. These modifications enhanced the stability of memory recall and facilitated the comprehension of complex patterns, underscoring critical role of neural maturation in enabling advanced recognition capabilities.

Recent technological progress in realizing human-like brain functions for recognizing objects, understanding natural language, and navigating behavior in systems like "self-driving cars," provided by artificial intelligence, has made a huge impact on our lives. These technologies continue to progress day by day. The basic model concepts of these artificial intelligences were provided by theoretical examinations of brain functions (1). Most of these theoretical bases were proposed before the expansion of molecular biology, indicating that major parts of the current astonishing progress in AI do not necessarily require an understanding of modern molecular biology.

There have been intense research efforts to reveal the molecular mechanisms of neuronal transmission "maturation" in neurophysiology, based on observations of developmental changes in the excitability of neurons through synaptic transmission. This is especially true for the Calyx of Held synapse, a brainstem relay neuron involved in hearing and sound localization (2). These changes collectively refine neural information delivery to higher processing regions of the brain (3-6). Because the function of the Calyx of Held is primarily the transmission of auditory information, a developmental shift towards "high fidelity" is certainly reasonable. At the same time, considering the general context of adult information processing compared to that of children, the hypothesis that neuronal transmission turns to high fidelity during development is quite generalizable in the brain.

Effect of pseudo-immature transmission in supervised and reinforced learning models

I speculated on the possibility of examining the significance of neural transmission maturation in conventional deep learning networks. First, I examined this in three-layer networks using supervised learning for the MNIST dataset (Fig. 1). I utilized ReLU for the activation function. This model network could learn text concepts immediately and maintain stable accuracy over long trials (Fig. 1A). I simply modified the forward transmission by adding random values to reproduce immature low-fidelity neural transmissions. Fig. 1B showed that this condition could also learn the concept, albeit with slightly lower accuracy. However, as a result of continuous learning, the obtained learning representation suddenly dropped off and was lost. This change caused a divergence in neural firing values. Therefore, I next examined clipping the activation function values at a certain point, such as limiting values over 500 to 500. Fig. 1C showed almost the same results as Fig. 1B. The last layer is directly converted to 0-9 text output. During the divergence of the value, when the true and false output layer values reached the limiting value, backpropagation couldn't recover the mismatch of input-output relations (data not shown). The results of random transmission with optimized learning rates using Adam, needed to adjust the learning rate lower than in the condition without Adam to maintain stable accuracy, but random transmission lost the stability of concept learning in the same way as the control condition (Fig. 1D and Fig. 1E). The results of utilizing random dropout also needed to adjust the learning rate slightly higher, but this condition yielded the same results as Fig. 1A and Fig.1B (Fig. 1F and Fig. 1G).

Then I examined the effects of random transmission in the reinforcement learning paradigm. I performed Q-Learning in a 3x4 grid world using a single-layer network. Fig. 2A shows the results of learning with the ReLU activation function. Compared with Fig. 2G (Step function), ReLU could have negative values, showing a higher variation of action functions. However, the ReLU function condition diverges the action function value due to random transmission (Fig. 1B). Under gradient-clipping conditions—where both gradient magnitudes and activation-

function outputs were capped at predefined limits—gradient divergence was suppressed even with random signal transmission; however, action learning was still inadequate, and the agent failed to achieve improved task navigation (Fig. 2D). In the case where ReLU activation function values over 10 are set to 0, causing the action function value to diverge nevertheless without adding randomness (Fig 2E). This was not observed when the value was clipped constantly (Fig. 2F). The condition where values over 50 are set to 0 did not induce the action function values to diverge (data not shown). On the other hand, in the Step function conditions (Fig. 2G and Fig. 2H), action function divergence was not observed even with random transmission. These results show that the ReLU type function is highly expressive but at the same time vulnerable to perturbations, whereas binary response functions are more stable.

KCNH7 - A candidate gene with higher expression in the mature mouse brain

I looked for a real molecular target contributing to neural firing fidelity. The simplest working hypothesis is that these genes would be expressed at higher levels in the adult brain compared to the immature brain. I searched for such potassium channels using the ALLEN BRAIN ATLAS DATA PORTAL (https://portal.brain-map.org/). From the in situ hybridization data of the developing mouse brain, I identified several candidates (Fig. 3A). Through the examination of the cell type database by single-cell RNA-Seq analysis (Fig. 3B), I selected KCNH7 as a good candidate.

The KCNH family comprises the ERG, EAG, and ELK voltage-activated, potassium-selective channels. These channels were originally identified as mutations in Drosophila that exhibited abnormalities under ether anesthesia (7). KCNH7 belongs to the ERG (Kv11) subfamily and due to their unique channel properties, Kv11 channels evoke greater conductance by hyperpolarization from depolarized potentials and regulate the resting membrane potential and action potential firing in neurons (8-10). According to the in situ hybridization data, KCNH7 starts to express at higher levels after P14 in the mouse telencephalic vesicle, midbrain, and medullary hindbrain (Fig. 3A). KCNH7 is clearly higher express in P56 Purkinje cell than P28. Fig. 3B shows samples from the P28 mouse brain, where KCNH7 is widely expressed throughout the cortex in both excitatory and inhibitory neurons. However, expression is partially low in some populations of CA3 and dentate gyrus neurons. In these cell types, the immature neuron marker Calbindin2 (Calretinin) is negatively correlated with KCNH7 expression, while the mature neuron marker Calbindin1 is positively correlated with KCNH7 expression (Fig. 3C) (11, 12). These results provide evidence for the potential importance of KCNH7 in adult neuron function.

Next, I examined the functions of KCNH7 in neurons. I utilized established neuron models by incorporating KCNH7 parameters. Niculescu et al. demonstrated the feasibility of inputting KCNH7 model parameters into a modified KGR model (10). I checked the channel kinetics through examinations such as activation and deactivation kinetics. My Hodgkin-Huxley-based model appeared to sufficiently reproduce the trends of KCNH7 parameters (Supplemental Table). Modified KGR models utilized in Niculescu et al. start to fire in a binary manner, meaning that adding threshold current induces continuous firing during the duration time (Fig. 4A). An increase in potassium channel conductance in the model induced a higher threshold in the neuron model, but the binary firing property remained unchanged (Fig. 4B). When KCNH7 model parameters were incorporated into this neuron model, the first firing threshold became higher, similar to the high potassium channel conductance model. The results showed that

KCNH7 strongly repressed the second firing, resulting in a continuous increase in the duration time of firing (Fig. 4C). This property aligns well with the reported physiological function of KCNH7 (10). This property could provide neural transmission fidelity in cases where transmission current varied near the set firing points (Fig. 4D left). The model including KCNH7 showed the same single action potential response even when slight perturbations occurred. One of the KCNH7 SNPs has been reported to be related to bipolar spectrum disorder (13). This amino acid replacement mutation shifts the KCNH7 V1/2 values to about +10mV higher threshold. This mutation parameter appears to partially block the KCNH7 function (Fig. 4D right) and provides insights into understanding the phenotype of this SNP.

I examined the above hypothesis through the activation of neurons by Poisson spike noise (Fig. 4E). I confirmed that KCNH7 suppressed variance caused by noise compared to the original model. This effect was partially impaired by the KCNH7 mutation. The high K channel conductance model also provided a similar effect, showing that the high threshold induced by these channels is important for stability under noise perturbation conditions. Then I examined the function of KCNH7 during high firing rate stimulation (Fig. 2F). The control neuron model couldn't maintain action potential firing at 530 Hz. Both the high conductance potassium channel and KCNH7 conditions maintained action potential firing at 530 Hz. KCNH7 showed a higher ability to sustain maximum firing response (150 Hz) even with high-frequency stimulation compared to high conductance potassium channel condtion(Fig. 4E simulation at 300Hz).

Effects of KCNH7 property in unsupervised learning models

I examined the significance of the property provided by KCNH7, which shifts the activation threshold higher, in a spiking neural network model using the STDP learning algorithm (14) (Fig. 5). The original development model is very stable even with long trial learning, as described in their work (Fig. 5 A; control). In High threshold condition, learning convergence was clearly slower than low threshold condition (Fig. 5 A; control). I perturbed the model by increasing the learning rate. Even under normal threshold conditions, the learned association firing was periodically lost during continuous learning. In low threshold conditions, where both excitatory and inhibitory neurons fire easily, this trend of learning loss increased further. On the other hand, the periodic drop in learning was partially suppressed in high threshold conditions. The difference is statistically significant ($p < 0.05$). These results potentially showed that the high threshold properties of neurons, achieved by increasing KCNH7 expression, provided stability for learning concepts.

Then, I examined the effect of randomness in unsupervised association learning using a Restricted Boltzmann Machine to generate the numbers of the MNIST dataset. I parameterized the temperature factor by dividing the sigmoid variable by the set temperature factor to control the randomness of information transmission during learning. Fig. 5B, C, and D show the results of character "5" concept learning and recalling by giving the test images. In this condition, ($t = 1$) (normal sigmoid function) was optimal (Fig. 5B). In low temperature conditions ($t = 1/4$), which induced binary-like activation, convergence was clearly fast (Fig. 5C). In high temperature and high randomness conditions ($t = 4$), the sigmoid was converted to a nearly linear function, where convergence was slow and divergence also occurred in some trials (Fig. 5D). These results are consistent with those in Fig. 1. However, when using the same paradigm for learning the characters "5" and "1," the convergence properties of the pair of numbers were opposite to the results above. In low temperature conditions ($t = 1/4$), convergence was still very

quick, but although the two-character concepts could be obtained initially, the learning concepts were rapidly lost, and eventually, only one character could be recalled (Fig. 5F). In 21 out of 150 tests, the maximum values reached over 0.6 accuracy, reflecting the ability to recall 2 characters, but in 0 tests did the accuracy remain over 0.6 at the last 400,000 epochs. This clearly showed a divergence of the concept. In high temperature conditions (t = 4), the two- character concepts gained higher accuracy as more trials were added. In 57 out of 150 tests, the maximum values reached over 0.6 accuracy, and in 49 tests, the accuracy remained over 0.6 at the last 400,000 epochs (Fig. 5G). These results show continuous convergence of the correct concepts. In the (t = 1) condition, 33 out of 150 tests had maximum values reaching over 0.6 accuracy, but only 14 tests maintained over 0.6 accuracy at the last 400,000 trials (Fig5E). Taken together, the results suggest that the linear response property provided by adding KCNH7 induces a higher capacity for complex information processing in neuronal function.

Direct Investigation into the Physiological Properties of Neural Maturation

I examined the direct influence of KCNH7 on network dynamics using a reservoir neural network built from a full-conductance Purkinje-cell model (its electrophysiological properties are characterized in Fig. 4). In the Mackey–Glass prediction task (Fig. 6A), introducing physiological levels of KCNH7 conductance enhanced prediction accuracy, whereas a two-fold increase in conductance degraded performance—presumably because it silenced firing too strongly. Consistently, the maximal Lyapunov exponent shifted from slightly positive (no KCNH7) to slightly negative (with KCNH7), indicating greater dynamical stability, and memory capacity reached its peak under normal conductance. When the same paradigm was applied to the KCNH7-mutant model (Fig. 4), the conductance level that yielded maximal performance was shifted upward. This shift was corroborated by parallel changes in the Lyapunov exponent and memory-capacity analyses, supporting the idea that KCNH7 modulates the trade-off between stability and representational power in a conductance-dependent manner.

Next, I examined the continuous learning trajectories for novel concept acquisition by analyzing two transient phases in each genotype across varying KCNH7 conductance levels (Fig. 6B). In the unstable WT condition (scale 2.0), the network initially adapts more quickly, but its inherently divergent dynamics slow the eventual convergence to a stable state. By contrast, the MUT network at the same 2.0 scale remains distinctly stable, suggesting that a physiological switch—likely modulated by the incoming signal—regulates proper stabilization of learning.

Finally, to determine how neural maturation influences the fidelity of cortical information processing, I analyzed in vivo two-photon Visual Behavior recordings (https://portal.brain-map.org/circuits-behavior/visual-behavior-2p) from mice aged P95–223 (Fig. 6C), capturing late-stage developmental changes. The participation ratio (PR) declined with age ($r = -0.30$, $p < 0.01$), whereas the activation time constant (τ) and behavioral sensitivity index d' remained stable across this period. Furthermore, PR correlated positively with d' ($r = 0.21$, $p < 0.05$) but showed no relationship with τ.

Robust regression confirmed a modest positive effect of PR on d' ($\beta = 0.12$, $p = 0.014$); however, this model explained less than 4% of the variance and was largely overshadowed by individual variability (ICC ≈ 0.48). Together, these findings suggest that representational dimensionality decreases during late-stage maturation primarily via network-level refinement rather than changes in intrinsic firing properties, and that preserving higher dimensionality may underpin enhanced behavioral performance.

Conclusions

Both supervised learning and reinforcement learning models showed that continuous learning trials under random conditions induced a loss of learning (Fig. 1 and Fig. 2). These losses were caused by the divergence of activation values. However, even when setting a limit on the activation value, similar to physiological neurons, these phenomena were still observed (Fig. 1C). Additionally, Fig. 2D showed that learning loss was still observed even when setting limits on the gradient. Fig. 2E and 2F suggest that firing failure has a more severe effect on learning establishment than maintaining maximal response frequency. The expression of KCNH7 could rescue this limitation of learning (Fig. 4F).

It seems that catastrophic forgetting is consistent with our results (15). It is induced by adding perturbations in learning sources, such as adding randomness in learning images. It is a straightforward interpretation that randomness in learning sources and transmission would have similar effects. Fig. 2 shows that learning loss due to randomness occurred only in the ReLU condition. It was also observed in supervised learning (data not shown). In the case of the step function (Fig. 2G), learning losses were not observed.

Regarding the complexities of learned behavior, ReLU had a higher variety of behavior possibilities. It could even learn “minus” parameters (Fig. 2A, shown in red). On the other hand, the step function only chose 0 or 1. Even with such low expression ability, the step function worked well and appeared to perform better than ReLU in this simple task and was at least clearly more robust to perturbations than ReLU. The same results could be obtained in the Restricted Boltzmann Machine model (Fig. 5A, 5b and 5C). In high temperature/high randomness conditions, the learning tended to lose its ability through continuous learning (Fig. 6C).

On the other hand, when the same Restricted Boltzmann Machine model learned a more complex context, the phenotype of learning loss became opposite. Low temperature conditions induced learning loss, while high temperature conditions provided stable, continuous improvement in learning accuracy (Fig. 5D, 5E, 5F).

These results provide a reasonable interpretation for the higher expression of KCNH7 in mature neurons (Fig. 3A). KCNH7 provides a continuous linear response and a higher threshold for neurons (Fig. 4C). In short, higher thresholds provide stability (Fig. 4E) in learning (Fig. 5A), and the complexity of responses gives the ability to handle complex problems (Fig. 5H and Fig. 5I). This could be seen as a simple expression of the maturation of intelligence in the adult brain, and moreover, it provides valuable insights into how to utilize such higher abilities in organizations and society.

Chronic treatments of adult mice with fluoxetine induce “dematuration” of mature granule cells through activation of 5HT-4 receptors (16). 5HT-4 receptors are known Gs-coupled receptors that activate PKA (17). Another group shows that 5HT-4 also activates PKC alpha in intestinal epithelial cells (18).

mGluR1, a Gq-coupled receptor, activation in Purkinje cells induces suppression of KCNH7 current, as measured by adding the ERG current inhibitor E4031, promoting excitation of neurons (10). This would disturb information stability as discussed here (Fig. 4E and Fig. 5A). Activation of mGluR1 coincidentally induced about a +10mV shift of KCNH7 V1/2. This might be the endogenous regulatory mechanism of KCNH7 through PKC phosphorylation. Indeed, KCNH7 is phosphorylated by PKC according to the KANPHOS database (https://kanphos.jp/).

Figs. 6A and 6B support this hypothesis. Endogenous modulation of G-protein-coupled receptors—such as serotonin and dopamine receptors—can attenuate potassium-channel conductance (19), thereby reshaping network dynamics. Our theoretical analysis suggests that nudging conductance toward an optimal balance enhances recognition performance; however, mis-coordinated plasticity can impair network function and contribute to disease. Accordingly, future therapeutic strategies should be guided by a careful investigation of the underlying molecular mechanisms.

Because of limited data availability, I could examine only a late-maturation window (postnatal day 95 and older). Within this stage I did not detect shifts in intrinsic firing properties that could be traced directly to potassium-channel changes, yet I still observed maturation-related stabilization of network activity—as indicated by a decline in participation ratio. Consistent with Fig. 5, higher behavioral performance also coincided with greater representational dimensionality. Although additional work is needed to link KCNH7 conductance definitively to network dynamics in vivo, these results highlight plausible routes—ranging from gene-expression levels and post-translational modifications to disease-associated mutations—through which KCNH7 dysregulation might contribute to disorders such as bipolar spectrum disorder.

Artificial intelligence is, of course, “artificial,” but recent progress in these technologies has already accomplished most human cognitive functions. The fact that most cognitive functions can be performed means that most cognitive functions can be approximately examined. Insights from AI can provide cues for understanding the significance of molecular mechanism dynamics in cognitive function, as shown here. My study is quite simple, and primitive compared to the deeper understanding of cognitive function mechanisms. Now, it is possible to build more sophisticated architectures of neural networks and to examine the same types of problems, surely making a huge breakthrough in the field.

Referecnce

1. Amari S. Backpropagation and stochastic gradient descent method. *Neurocomputing* **5**, 185-196 (1993).

2. Takahashi T. Strength and precision of neurotransmission at mammalian presynaptic terminals. *Proceedings of the Japan Academy Series B* **91**, 305-320 (2015).

3. Koike-Tani M, Saitoh N, Takahashi T. Mechanisms Underlying Developmental Speeding in AMPA-EPSC Decay Time at the Calyx of Held. *J Neurosci.* **25**, 199-207 (2005).

4. Taschenberger H and von Gersdorff H. Fine-Tuning an Auditory Synapse for Speed and Fidelity: Developmental Changes in Presynaptic Waveform, EPSC Kinetics, and Synaptic Plasticity. *J neurosci.* **20**, 9162-73 (2000).

5. Yamashita T, Eguchi K, Saitoh N, von Gersdorff H, Takahashi T. Developmental shift to a mechanism of synaptic vesicle endocytosis requiring nanodomain Ca2+. *Nat Neurosci.* **13**, 838–844 (2010).

6. Yang YM and Wang LY. Amplitude and Kinetics of Action Potential-Evoked Ca2+ Current and Its Efficacy in Triggering Transmitter Release at the Developing Calyx of Held Synapse. *J Neurosci.* **26**, 5698–5708 (2006).

7. Brüggemann A, Pardo LA, Stühmer W, Pongs O. Ether-à-go-go encodes a voltage-gated channel permeable to K+ and Ca2+ and modulated by cAMP. *Nature* **365**, 445-8 (1993).

8. Perry M, Sanguinetti M, Mitcheson J. Revealing the structural basis of action of hERG potassium channel activators and blockers. *J Physiol.* **588**, 3157-67 (2010).

9. Akbarali HI, Thatte H, He XD, Giles WR, Goyal RK. Role of HERG-like K(+) currents in opossum esophageal circular smooth muscle. *Am J Physiol.* **277**, C1284-90 (1999).

10. Niculescu D, Hirdes W, Hornig W, Pongs O, Schwarz JR. Erg Potassium Currents of Neonatal Mouse Purkinje Cells Exhibit Fast Gating Kinetics and Are Inhibited by mGluR1 Activation. *J Neurosci.* **33**, 16729-40 (2013).

11. Iacopino AM, Rhoten WB, Christakos S. Calcium binding protein (calbindin-D28k) gene expression in the developing and aging mouse cerebellum. *Brain Res Mol Brain Res.* 8, 283-90 (1990).

12. Brandt MD, Jessberger S, Steiner B, Kronenberg G, Reuter K, Bick-Sander A, von der Behrens W, Kempermann G. Transient calretinin expression defines early postmitotic step of neuronal differentiation in adult hippocampal neurogenesis of mice. *Mol Cell Neurosci.* **24**, 603-13 (2003).

13. Strauss KA, Markx S, Georgi B, Paul SM, Jinks RN, Hoshi T, McDonald A, First MB, Liu W, Benkert AR, Heaps AD, Tian Y, Chakravarti A, Bucan M, Puffenberger EG. A population-based study of KCNH7 p.Arg.394His and bipolar spectrum disorder. *Mol Genet.* **23**, 6395-406 (2014).

14. Diehl PU, Cook M. Unsupervised learning of digit recognition using spike-timing-dependent plasticity. *Front Comput Neurosci.*, 9:99 (2015).

15. Kirkpatricka J, Pascanua R, Rabinowitza N, Venessa J, Desjardinsa G, Rusua AA, Milana K, Quana J, Ramalhoa T, Grabska-Barwinskaa A, Hassabisa D, Clopathb C, Kumarana D, Hadsella R. Overcoming catastrophic forgetting in neural networks. *Proc Natl Acad Sci USA*. **114**, 3521-3526 (2017).

16. Kobayashi K, Ikeda Y, Sakai A, Yamasaki N, Haneda E, Miyakawa T, Suzuki H. Reversal of hippocampal neuronal maturation by serotonergic antidepressants. *Proc Natl Acad Sci USA.* **107**, 8434-9 (2010).

17. Torres GE, Arfken CL, Andrade R. 5-Hydroxytryptamine4 receptors reduce afterhyperpolarization in hippocampus by inhibiting calcium-induced calcium release5-Hydroxytryptamine4 receptors reduce afterhyperpolarization in hippocampus by inhibiting calcium-induced calcium release. *Mol Pharmacol.* **50**, 1316-22 (1996).

18. Gill RK, Saksena S, Tyagi S, Alrefai WA, Malakooti J, Sarwar Z, Turner JR, Ramaswamy K, Dudeja PK. Serotonin inhibits Na+/H+ exchange activity via 5-HT4 receptors and activation of PKCα in human intestinal epithelial cells. *Gastroenterology* **128**, 962-74 (2005).

19. Tsuboi D, Otsuka T, Shimomura T, Faruk MO, Yamahashi Y, Amano M, Funahashi Y, Kuroda K, Nishioka T, Kobayashi K, Sano H, Nagai T, Yamada K, Tzingounis AV, Nambu A, Kubo Y, Kawaguchi Y, Kaibuchi K. Dopamine drives neuronal excitability via KCNQ channel phosphorylation for reward behavior. *Cell Rep.*, **40**, 111309 (2022).

20. Kozareva V, Martin C, Osorno T, Rudolph S, Guo C, Vanderburg, Nadaf N, Regev A, Regehr WG, Macosko E. A transcriptomic atlas of mouse cerebellar cortex comprehensively defines cell types. *Nature* **598**, 214-219 (2021).

Acknowledgments:

I am thankful for the kind support of Junichiro Yoshimoto for discussions and comments on my work. Hiroshi Watanabe, Yukihiro Nakamura and Atsuhito Toyomaki also provided comments and support for my work.

Competing interests:

The author declares no competing interests.

Data and Code Deposition:

All analytical code in the main text and Supplementary Materials is available in the GitHub repository at https://github.com/BreamResearch/Neural-Maturation, which will be made public upon acceptance of this article.

Fig. 1. Effect of pseudo-immature transmission in supervised learning model

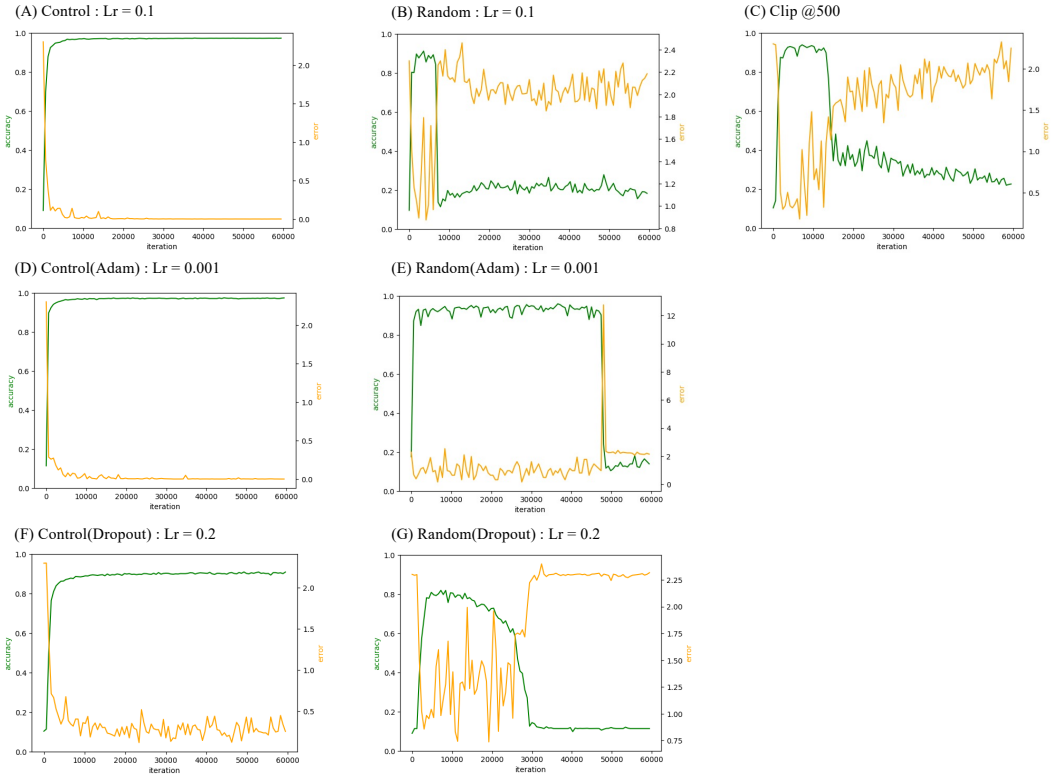

Fig. 1. Effect of pseudo-immature transmission in supervised learning model

The MNIST text recognition task was performed using a typical deep layer network for supervised learning. The basic architecture and algorithm are described in the link (https://github.com/oreilly-japan/deep-learning-from-scratch). I modified the 784-50-10 network to a 784-50-50-10 network. A random value between 0.1 and 1 was added in the ReLU function process. In the clipped condition, the ReLU output value was clipped at 500, and any differential value above 500 was set to 0. The green line shows the accuracy of recognition (left vertical axis), and the orange line shows the loss value (right vertical axis). The horizontal axis shows the iteration numbers. (A) Control. The learning rate is 0.1. (B) Random forward (Pseudo-immature) transmission. (C)Random transmission with ReLU activation value was clipped at 500. (D) Using Adam optimization and with random transmission (E). The learning rate is 0.001. (F) Using random dropout and with random transmission (G). The learning rate is 0.2.

Fig. 2. Effect of pseudo-immature transmission in reinforced learning model

(A) Control

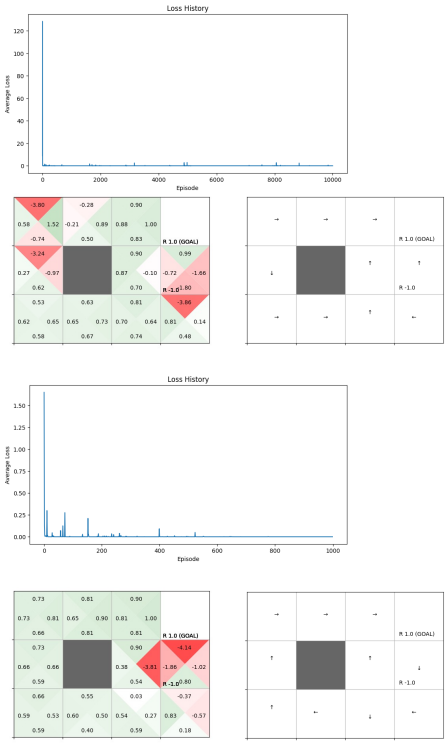

(B) Random

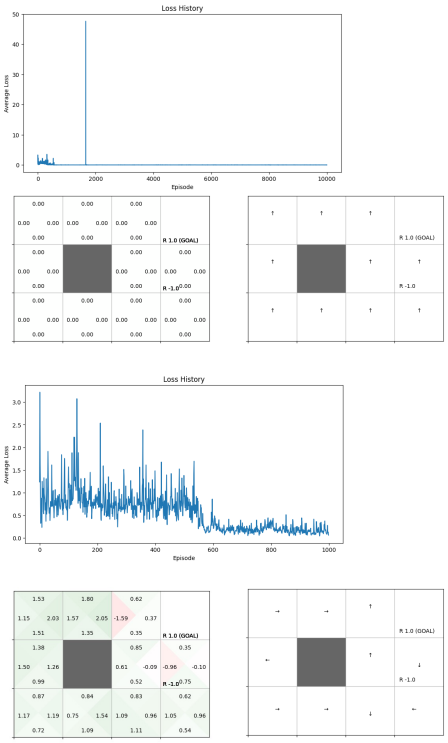

(C) Grad clipping

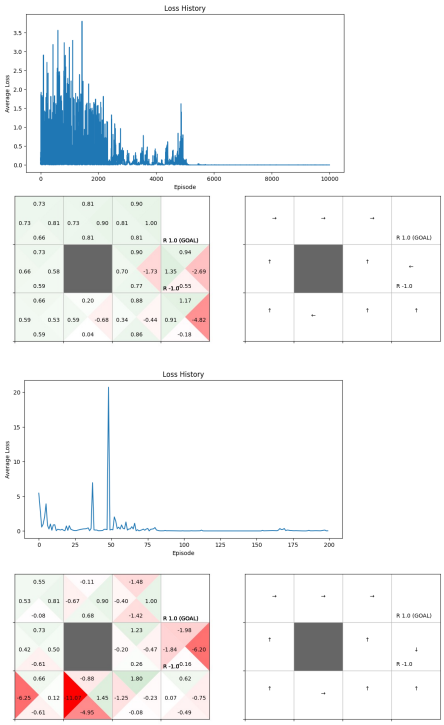

(D) Grad clipping + Random

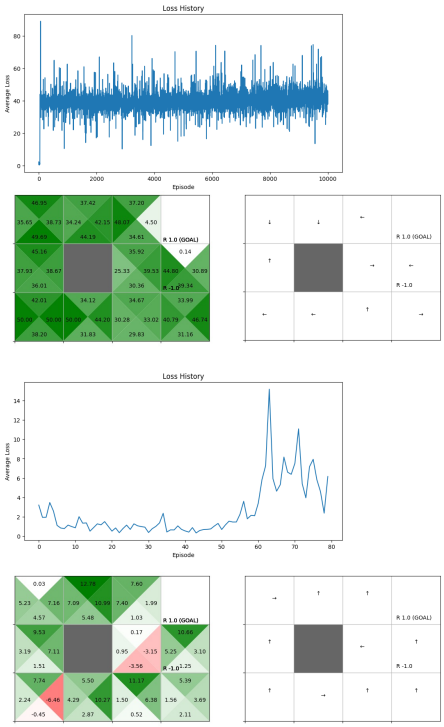

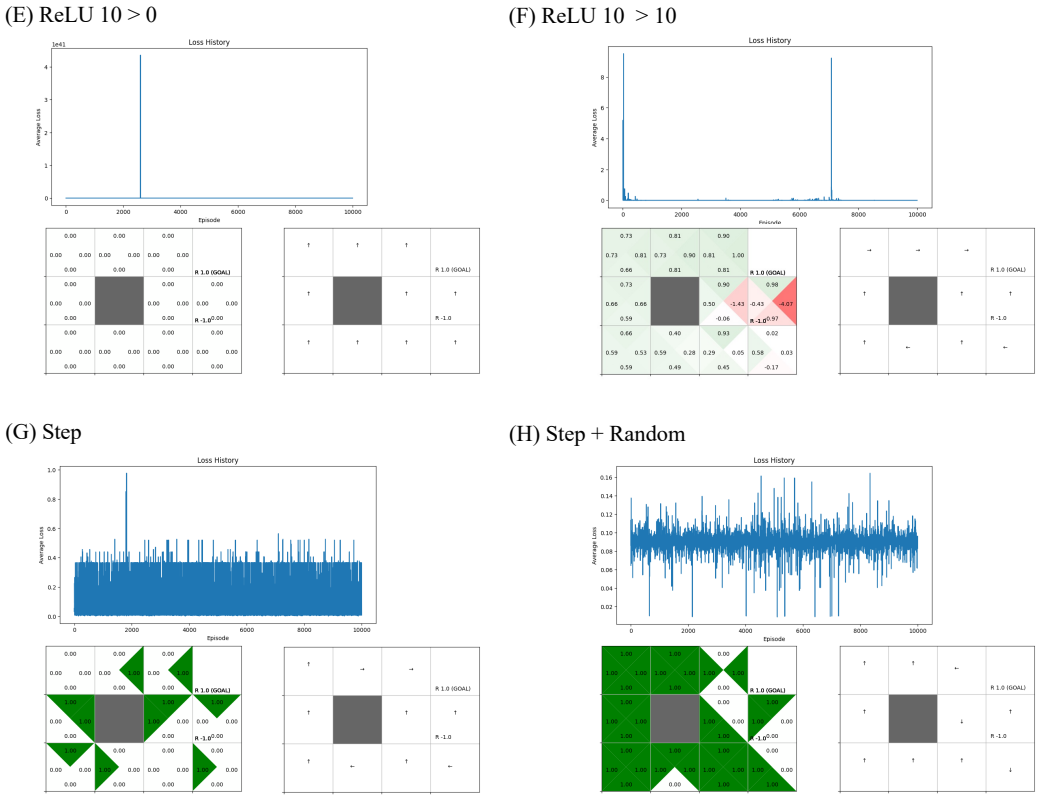

Fig. 2. Effect of pseudo-immature transmission in reinforced learning model

3x4 maze tasks were performed using Q-Learning. The basic architecture and algorithm are described in the link (https://github.com/oreilly-japan/deep-learning-from-scratch-4). The behavioral strategy was learned by a single-layer network. A random value between 0.65 and 1 was added to the forward transmission. The ReLU output value was clipped at 50. In the gradient clip condition, the gradient was clipped at 5. The step function sets values over 0.5 to 1. Briefly, the agent starts from the bottom left block and chooses the next action based on the expectation value. If the agent hits the wall, it stays in place without incurring a penalty. When the agent reaches the goal reward point, it returns to the starting point and begins the next episode. The vertical axis shows the loss value, and the horizontal axis shows the episode numbers. The subplot shows the value of actions chosen in each block and the typical action directions for the next steps. (A) Activation function was ReLU. The activation function values was clipped at 50 for avoiding gradient explosion. (B) Random forward transmission with ReLU. (C) Gradient max value clipped at 5 and its random transmission(D). (E) ReLU activation values over 10 are set to 0, or 10 (F). (G)Step function and with random transmission (H).

Fig. 3. Candidate potassium channels expressed at higher levels in mature neurons

(A) In situ hybridization

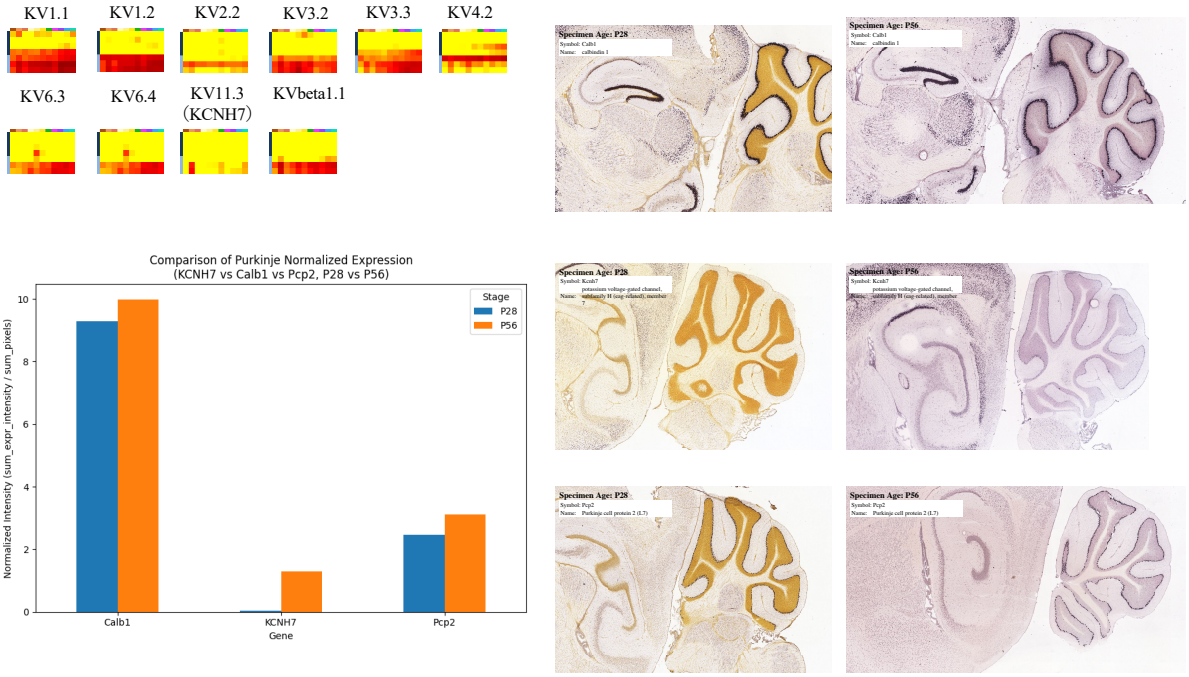

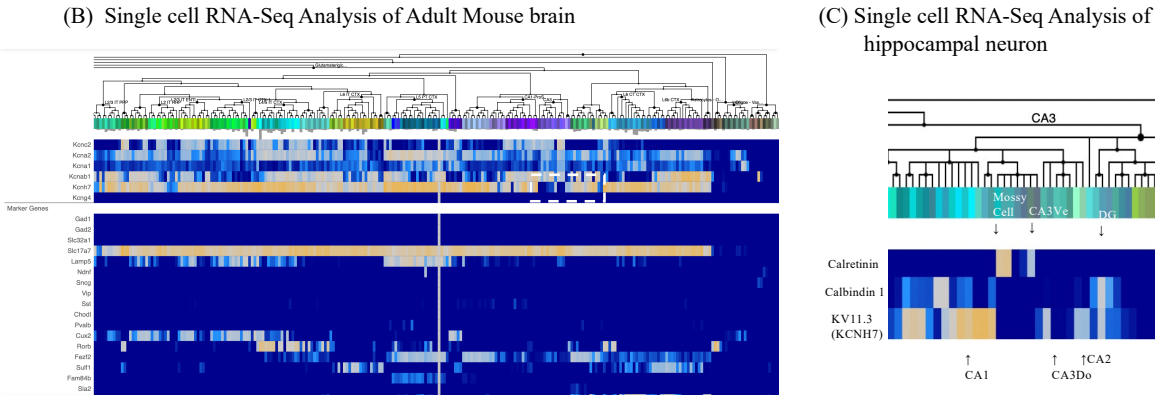

Fig. 3. A candidate gene with higher expression in the mature mouse brain

Explore develop dependent up-regulating potassium channels in ALLEN BRAIN MAP. (A) In situ hybridization of mouse brain in each developmental stage and regions (https://developingmouse.brain-map.org/gene/show/82041). Vertical axis shows developmental stage, E11.5, E13.5, E15.5, E18.5, P4, P14 and P28. Horizontal axis shows brain regions, RSP, Tel, PedHy, p3, p2, p1, M, PPH, PH, PMH and MH. Right shows in situ hybridization of KCNH7 in P28 and P56 mouse cerebellum. As showed previously, KCNH7 was seen only expressed in Purkinje cell (20). Signal analysis of Purkinje cell clearly show upregulation of KCNH7 through neural maturation. (B) Single cell RNA-Seq analysis of adult, P28, mouse brain (https://celltypes.brain-map.org/rnaseq/mouse_ctx-hpf_10x?selectedVisualization=Heatmap&colorByFeature=Cell+Type&colorByFeatureValue=Gad1). (C) The white dashed line area in (B) shows KCNH7 expression in hippocampal neurons.

Fig 4. Functions of KCNH7 for neural fidelity and linear responses

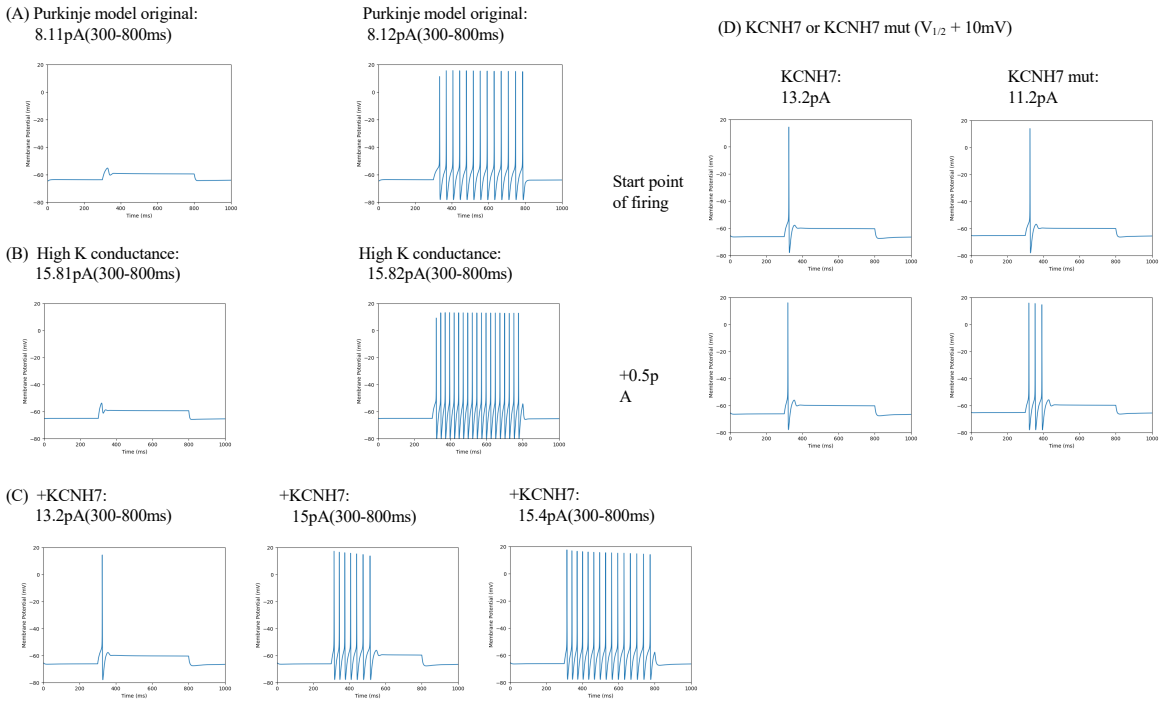

(E) Effect of noise in the models

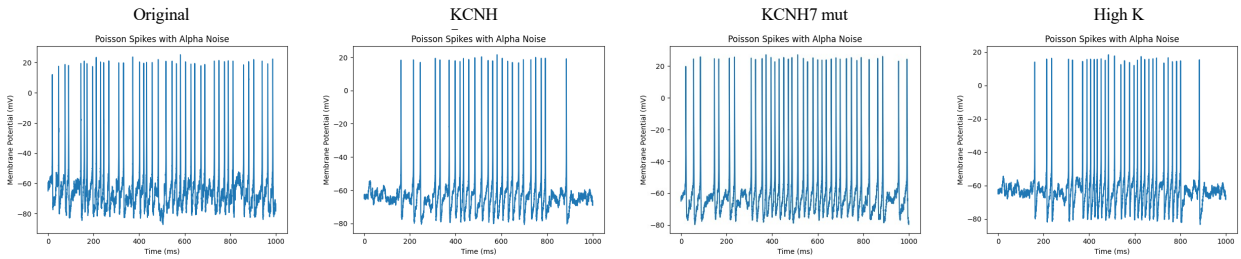

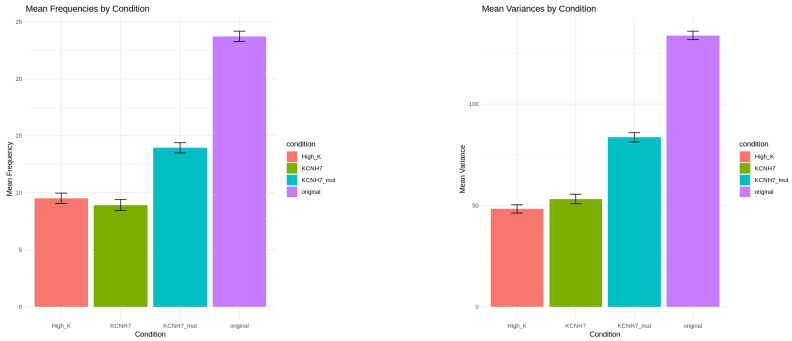

(F) KCNH7 suppresses failing of action potential

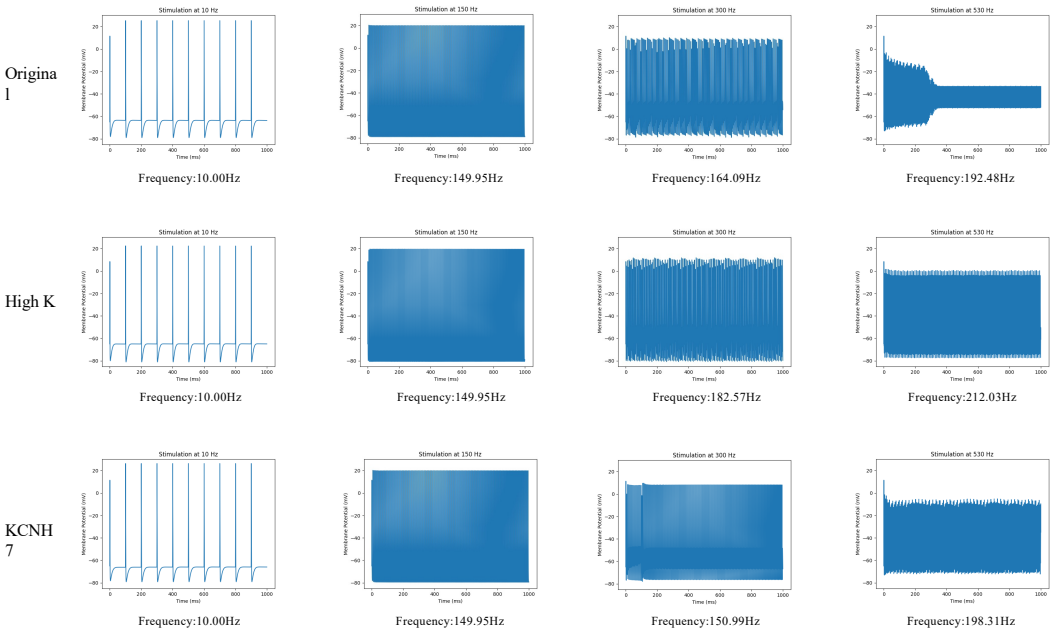

Fig. 4. Functions of KCNH7 for neural fidelity and linear responses

Examine the effects of KCNH7 parameter insertion in Purkinje cell model. The KCNH7 neuron was simulated using the NEURON simulator (https://www.neuron.yale.edu/neuron/). The basic Purkinje model and KCNH7 parameters were taken from Niculescu et al.. The KCNH7 kinetics parameters were estimated based on the protocol described in their work (10). Neuron models were stimulated from 300ms to 800ms at indicated amplitudes. (A) The threshold point for firing in the original model. (B) Increased potassium channel conductance in the model. (C) Inserted KCNH7 parameter as reported previously.(D) Comparison of KCNH7 and pseudo-mutant with a +10mV higher V half, near the thresholds. (E) Effect of random noise. Each simulation model was added Poisson spikes and noise. The upper part shows the example of responses of the spikes. The lower part shows the mean values of frequency and variance from 50 seed trials. Except between KCNH7 and High K, all pairs showed statistically significant differences in both. The error bars are shown in the figure. (F) Comparison of the above three neurons under 10, 150, 300, and 530 Hz action potential-like stimulation.

Fig. 5. Effect of KCNH7 Properties on Unsupervised Learning Models

(A) Spiking neural network model

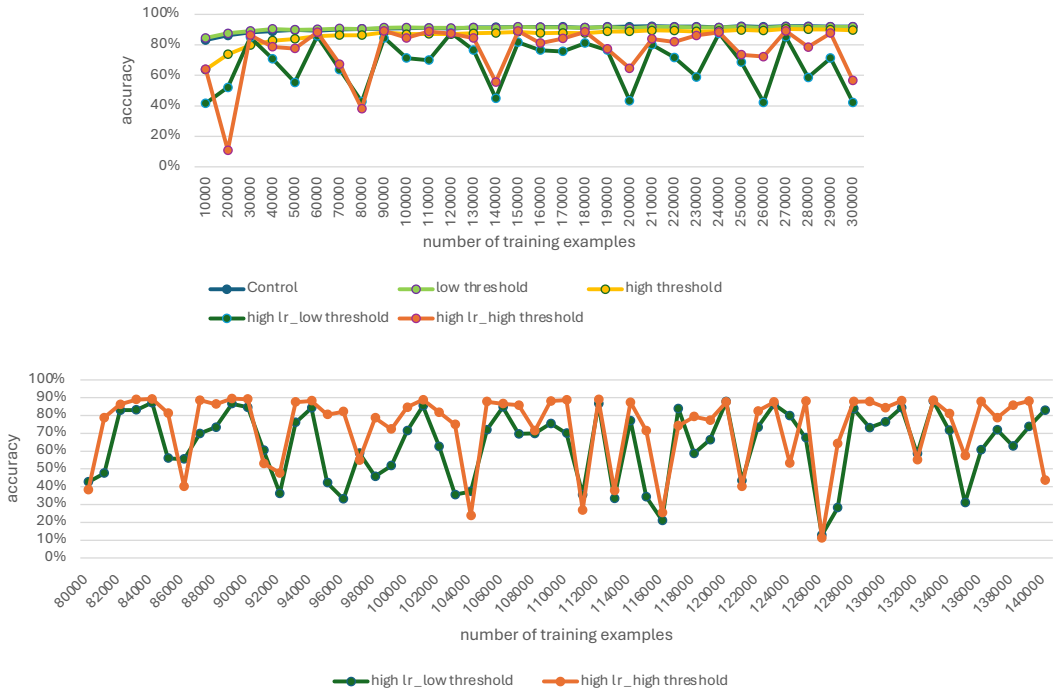

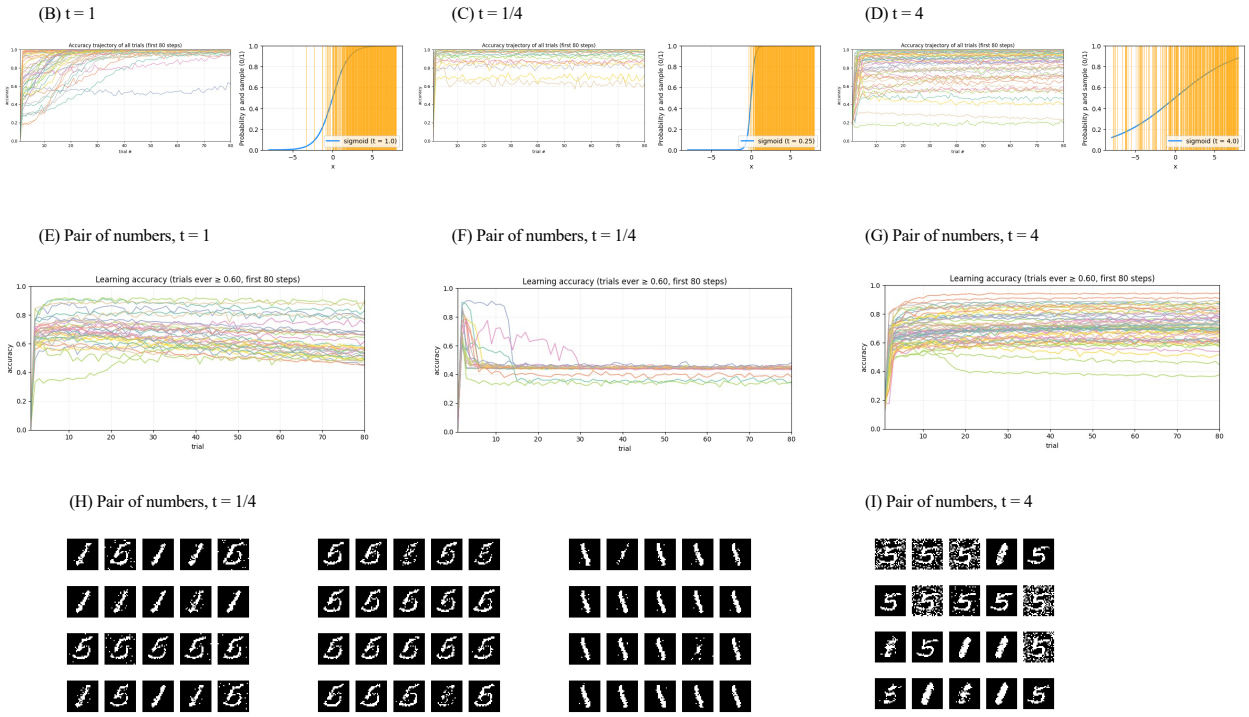

Fig. 5. Effects of KCNH7 property in unsupervised learning models

The basic architecture and algorithm are described in Diehl and Cook (14). I modified the learning rate and firing thresholds for both excitatory and inhibitory neurons. The low threshold condition is -62mV for excitatory neurons and -44mV for inhibitory neurons. The high threshold condition is -42mV for excitatory neurons and -35mV for inhibitory neurons. The vertical axis represents the proportion of concordant firing neurons between the training and test sessions, while the horizontal axis denotes the number of trials. (a)Comparison of each condition in normal and 70 times higher Learning rate (Lr). The control condition represents the optimal setting from the original paper. Lower panel; higher Learning rate, tested every 1,000 trials. (b)Numeric text recall from the MNIST dataset by a Restricted Boltzmann Machine. The MNIST dataset was learned using a 784-256 network Restricted Boltzmann Machine. A set of 5000 characters from the training dataset was used for learning and updating values using the Contrastive Divergence (CD) method. After training on the 5000-character dataset, evaluation tests were performed, repeating this process up to 80 times, totaling 400,000 trials. All test characters from each number were used for recalling character concepts, and the generated characters were discriminated by a supervised learning model as shown in Figure 1. Temperature parameters in both forward transmission and random sampling were set to 1 (B), 1/4 (C), and 4 (D). The accuracy of text recall was calculated by the trained supervised learning network in Fig. 1. The vertical axis shows accuracy, and the horizontal axis shows the number of test trials (5000 epochs of additional learning in each trial, totaling 400,000 epochs). The right shows sigmoid shapes (blue) and firing probabilities of sampling (orange) for each t and x value. (E), (F), and

(G) show the results of learning pair of numbers (5 and 1) and examples of generated characters. I selected data that achieved over 0.6 accuracy at the maximum during the trial. (H) The examples of generative characters in (F). Initially, two character concepts were obtained but were lost through continuous learning trials (left and center). The right image shows an example where one character concept was obtained. (G) The examples of generative characters in (I) showing two character concepts obtained.

Fig. 6. Direct Investigation into the Physiological Properties of Neural Maturation

(A) Mackey–Glass Time Series Predictions

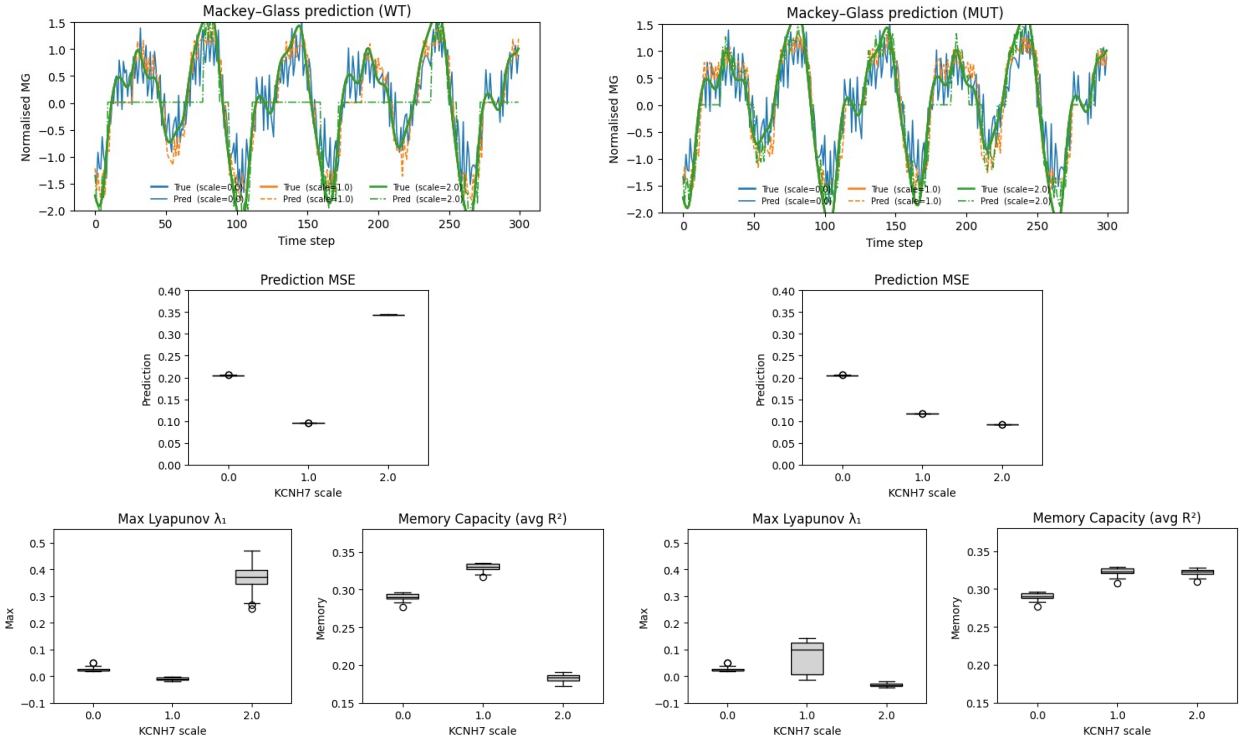

(B) Two Phase learning

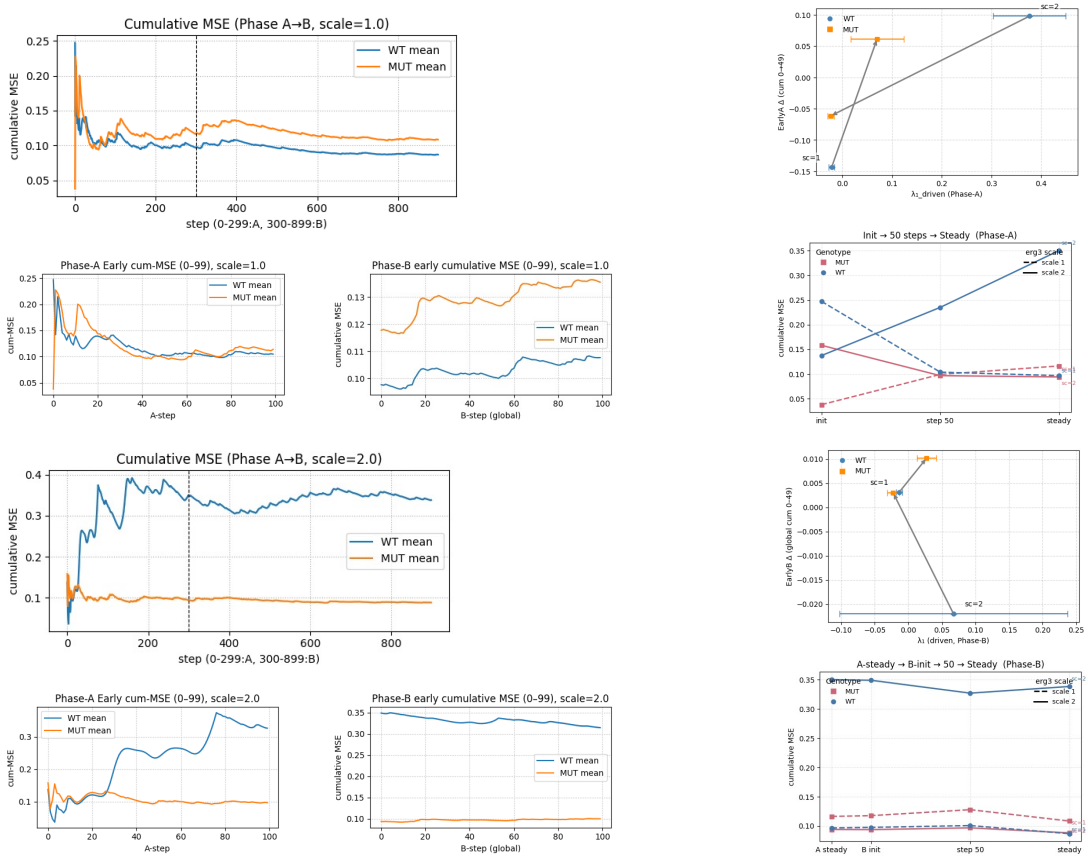

(C) Visual Behavior 2-Photon (VB2P) data analysis

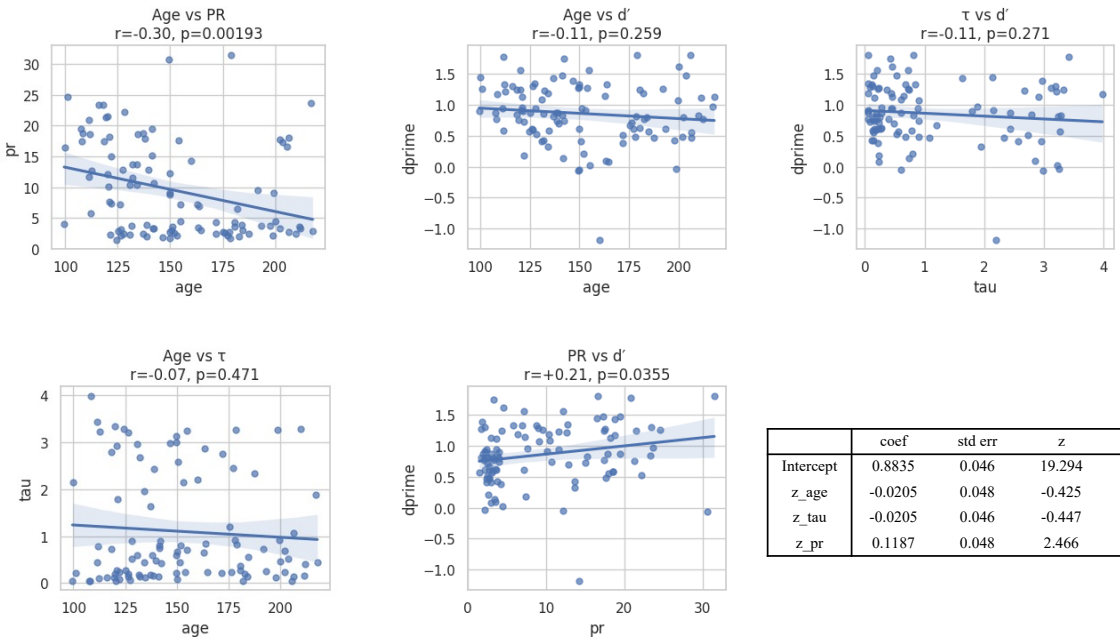

	coef	std err	z	P>|z|
Intercept	0.8835	0.046	19.294	0
z_age	-0.0205	0.048	-0.425	0.671
z_tau	-0.0205	0.046	-0.447	0.655
z_pr	0.1187	0.048	2.466	0.014

Fig. 6. Direct Investigation into the Physiological Properties of Neural Maturation

(A) A reservoir neural network was constructed from a Purkinje-cell conductance model. The network comprised 200 neurons (50 % excitatory, 50 % inhibitory) connected recurrently with random synaptic delays. Each neuron received background Poisson spiking to sustain intrinsic activity in the absence of external input. A 1200-step Mackey–Glass time series was generated; the first 800 steps were used for on-line delta-rule training, followed by a 100-step washout and a 300-step prediction phase. Results are reported as the mean ± SEM across 30 independent random seeds. Lower panel: The maximal Lyapunov exponent was estimated from the first two principal-component projections of the reservoir state, averaged over the time points that explained ≥ 95 % of the variance while the reservoir was driven by the Mackey–Glass input. To quantify how much past input the reservoir retained, we used the standard delay-line memory-capacity (MC) metric. After the 100-step washout, reservoir states were recorded for 500 + 20 samples. For each delay (1–20 steps) we built input–output pairs and fitted ridge-regression models with stratified five-fold shuffle cross-validation. The coefficient of determination (R^2) on each held-out fold was computed, and MC was defined as the mean R^2 across all valid (delay, fold) combinations. Right show the same analysis performed with the KCNH7-mutant channel characterized in Fig. 4. (B) Continuous plots of the Phase-A and Phase-B Mackey–Glass learning profiles, accompanied by magnitude plots that highlight early-phase learning in each phase. The right-hand panel shows the transient catch-up during the initial phases, plotted against the maximum Lyapunov exponents for each genotype and the corresponding KCNH7 conductance levels. (C) Visual Behavior 2-Photon (VB2P) data (OPHYS 1–6 imaging sessions)

were obtained via the AllenSDK. Sessions containing at least 10 cells and 10 trials were retained, yielding 1063 sessions from 101 unique mice. All variables were z-scored within each mouse to remove inter-individual baselines, and multivariate relationships were assessed with Huber-robust regression.